

TWO-AND THREE-DIMENSIONAL TRANSIENT RESPONSES OF HALF-SPACE UNDER DYNAMIC STRIP LOADS AND TRAIN TRACK LOADS

Maher ADAM¹, Gero PFLANZ² And Günther SCHMID³

SUMMARY

Two modelling approaches for the analyses of half-space subjected to dynamic loads are presented. A three-dimensional modelling is performed by means of the Boundary Element Method (BEM) and a two-dimensional one using a coupled Boundary Element - Finite Element method (BE-FE). The comparison between the results of the presented methods points out that the problem at hand can be treated as two-dimensional if the length to width ratio is not less than 3. For ratios less than 1.5, the problem has to be treated as three-dimensional. As an application, a parameter study of a wave propagation problem in a train track model is presented.

INTRODUCTION

The ground vibration caused by rail traffic has increased considerably during the last three decades leading to several environmental consequences. For instance, heavy axle trains running at low speed give rise to surface wave propagation to the nearby buildings. The main component of such vibrations lies in the frequency range of about 4 Hz to 50 Hz. The waves propagating at the low end of this frequency range may interact with the natural vertical modes of vibration of the nearby buildings. On the other hand, vibrations in the frequency range from about 50 Hz to 200 Hz which are mainly associated with trains running in tunnels, excite the bending resonance of walls and floors in buildings which then radiate noise directly into their interior. Surface running light rail vehicles which pass close to buildings can also cause unacceptable levels of rumbling noise. Recently, with the expansion of high speed passenger train networks, concern has been raised about the effect of moving loads on the track and embankment structure. It is thus important to study these phenomena theoretically in order to present engineering solutions which reduce their impact on the environment. Since there are a number of effects of vibration related to wave propagation, it is not surprising that a range of different modelling approaches are applied. Two-dimensional models have been used to study vibrations and wave propagation in soils due to train passage [Chu et al, 1992, Jones, 1994, Jones and Block, 1996]. To study the effects of the high speed moving loads, a three-dimensional model is essential [Krylov, 1995, Yoshioka and Ashiya, 1990, Pflanz, 1999]. In this paper, two modelling approaches are presented to investigate the dynamic response and wave propagation through the train track embankment to the underlying half-space. The three-dimensional modelling uses the Boundary Element Method (BEM). The two-dimensional modelling employs the coupled Boundary Element - Finite Element (BE-FE) method. In both approaches, the radiation conditions are fulfilled and no absorbing boundary conditions have to be introduced. First, the validity of each approach is demonstrated using results from literature. Second, the responses of a half-space due to vertical and horizontal impulse line loads are obtained by both methods and compared. Last, a parameter study of the wave propagation in the track embankment and the underlying half-space to the nearby soil surface is performed.

ANALYTICAL AND NUMERICAL APPROCHES

Boundary Integral Formulation

Assuming a homogeneous, isotropic, linear elastic medium, the equation of motion is expressed as:

¹ Department of Civil Engineering, Zagazig University, Cairo, Egypt. Email: mariadam@frcu.eun.eg, Fax: +(20) 13-601-510

² Graduiertenkolleg Ruhr University Bochum, Germany. Email: pflanz@sim.bi.ruhr-uni-bochum.de

³ Department of Civil Engineering, Ruhr University Bochum, Germany. Email: schmid@sim.bi.ruhr-uni-bochum.de

$$(c_1^2 - c_2^2)u_{,k,ki} + c_2^2 u_{,i,kk} - \ddot{u}_i + f_i = 0, \quad i, k = 1, 2, 3 \quad (1)$$

where commas and dots indicate space and time derivatives, respectively, and $u_i(\mathbf{x}, t)$ describes the three-dimensional displacement field. The constant parameters c_1 and c_2 represent the dilatational and the shear wave velocities, respectively, and f_i represents the body forces at each point in the domain Ψ . The initial and boundary conditions that have to be satisfied are given as:

$$u_i(\mathbf{x}, t=0) = u_i^0(\mathbf{x}), \quad \dot{u}_i(\mathbf{x}, t=0) = v_i^0(\mathbf{x}) \quad \forall \quad \Psi + \Gamma \quad (2)$$

$$u_i(\mathbf{x}, t) = \bar{u}_i(\mathbf{x}, t) \quad \forall \quad \mathbf{x} \in \Gamma_1, \quad t_i(\mathbf{x}, t) = \sigma_{ik} n_k = \bar{t}_i(\mathbf{x}, t) \quad \forall \quad \mathbf{x} \in \Gamma_2 \quad (3)$$

where $\Gamma = \Gamma_1 \cup \Gamma_2$ is the boundary of the domain Ψ , t_i represent the traction and n_i are the direction cosines of the outward normal to the boundary. The fundamental solution of equation (1), that is, the response of an infinite medium to a unit impulse at time τ in the direction x_k and located at point ξ is given by [Stokes, 1849]:

$$u_{ik}^*(\mathbf{x}, t, \xi, \tau) = \frac{t-\tau}{4\pi\rho r^2} \left\{ \frac{3r_i r_k - \delta_{ik}}{r} \left[H\left(t-\tau-\frac{r}{c_1}\right) - H\left(t-\tau-\frac{r}{c_2}\right) \right] + \frac{r_i r_k}{c_1} \delta\left(t-\tau-\frac{r}{c_1}\right) + \frac{\delta_{ik} - r_i r_k}{c_2} \delta\left(t-\tau-\frac{r}{c_2}\right) \right\} \quad (4)$$

where H is the Heaviside function, r denotes the distance $|\mathbf{x} - \xi|$ between the field point \mathbf{x} and the source point ξ , r_i is expressed by $r_i = x_i - \xi_i$ and u_{ik}^* describes the displacement of the field point \mathbf{x} in the direction x_i . The fundamental solution in equation (4) has the properties of reciprocity, time translation, and causality [Mansur and Brebbia, 1982]. Taking the source point ξ to the boundary yields, in the absence of body forces, the following boundary integral equation:

$$c_{ik} u_k(\xi, t) = \int_{\Gamma_1} u_{ik}^*(\mathbf{x}, t, \xi, \tau) t_i(\mathbf{x}, \tau) d\Gamma_x - \int_{\Gamma_2} t_{ik}^*(\mathbf{x}, t, \xi, \tau) u_i(\mathbf{x}, \tau) d\Gamma_x \quad (5)$$

where the boundary matrix c_{ik} includes the integral-free terms [Gaul, 1998].

Three-dimensional BEM

The boundary integral equation (5) is solved numerically by space and time discretization. The boundary Γ is divided into space boundary elements and the time domain is discretized using a linear interpolation function for displacement and a constant one for traction. The time integration is performed analytically, then, the numerical integration using *Gaussian* quadrature takes place. In the first time step, particular techniques have to be applied for quadrature, because of the singularity in the boundary integral kernels. The traction kernel has a strong singularity and the corresponding integral exists as a principal value, whereas the displacement kernel has a weak singularity, and the regular integration is enough. However, particular techniques are required as well to obtain higher accuracy with a lower number of *Gaussian* points. To integrate the weak singular kernels, a transformation on triangular polar coordinates is used. For the strong singular traction kernels, an additional Taylor-series expansion of the singular terms is employed [Li and Gue-Ming, 1985, Guiggiani 1992]. Using constant interpolation functions in the space domain, the system of linear equations takes the following form

$$c_{ik} u_i(\xi, t_N) + \sum_{l=1}^L \sum_{m=1}^N \int_{\Gamma_l} {}^0 T_{ik}^{(N-m+1)}(\mathbf{x}, \xi) d\Gamma_{lx} {}^{(l)} u_i^{(m)} + \sum_{l=1}^L \sum_{m=1}^N \int_{\Gamma_l} {}^1 T_{ik}^{(N-m+1)}(\mathbf{x}, \xi) d\Gamma_{lx} {}^{(l)} u_i^{(m-1)} \\ = \sum_{l=1}^L \sum_{m=1}^N \int_{\Gamma_l} {}^0 U_{ik}^{(N-m+1)}(\mathbf{x}, \xi) d\Gamma_{lx} {}^{(l)} t_i^{(m)} \quad (6)$$

where T_{ik} and U_{ik} are the fundamental solution temporal integrals. The outer summation is carried out over the total number of elements L and the inner one is carried out up to the current time step N . The free term coefficients c_{ik} are evaluated analytically [GAUL, 1998]. Equation (6) can be written in a matrix form as

$$\mathbf{U}^1 \mathbf{t}^N = \mathbf{T}^1 \mathbf{u}^N + \mathbf{E}^N, \quad \mathbf{E}^N = \sum_{m=2}^N \mathbf{T}^m \mathbf{u}^{N-m+1} - \mathbf{U}^m \mathbf{t}^{N-m+1} \quad (7)$$

where \mathbf{U}^m and \mathbf{T}^m are the coefficient matrices of the system at time $m\Delta t$. For the current time step N , all traction vectors \mathbf{t}^m , $m = 1$ to N , and previous displacement vectors \mathbf{u}^m , $m = 1$ to $N-1$, are known.

Two-dimensional Coupled BE-FE Method

In this approach, the problem will be divided into two parts. The uniform half-space is modeled by boundary elements and the non-homogenous part of soil, embankment, dam, structure, etc., is modeled by finite elements. The compatibility and equilibrium conditions should be satisfied along the common interface. It should be noted that the integral representation in equation (5) holds on the same form for both three- and two-dimensional problems. For a two-dimensional problem, the domain Ψ reduces to a plane region, the boundary Γ reduces to a closed curve, the fundamental solution corresponds to a unit line impulse load, and the subscripts i, k take the values of 1 and 2 only. Therefore, the above three-dimensional BEM formulation is also valid for the current two-dimensional formulation with minor changes. Denoting the interface node variables by the subscript i and the others by o , the governing equation of motion of a finite element domain due to a time dependant applied load $\mathbf{P}(t)$ can be expressed for the current time step N :

$$\begin{bmatrix} \mathbf{M}_{oo} & \mathbf{M}_{oi} \\ \mathbf{M}_{io} & \mathbf{M}_{ii} \end{bmatrix} \begin{Bmatrix} \ddot{\mathbf{u}}_o \\ \ddot{\mathbf{u}}_i \end{Bmatrix}^N + \begin{bmatrix} \mathbf{C}_{oo} & \mathbf{C}_{oi} \\ \mathbf{C}_{io} & \mathbf{C}_{ii} \end{bmatrix} \begin{Bmatrix} \dot{\mathbf{u}}_o \\ \dot{\mathbf{u}}_i \end{Bmatrix}^N + \begin{bmatrix} \mathbf{K}_{oo} & \mathbf{K}_{oi} \\ \mathbf{K}_{io} & \mathbf{K}_{ii} \end{bmatrix} \begin{Bmatrix} \mathbf{u}_o \\ \mathbf{u}_i \end{Bmatrix}^N = \begin{Bmatrix} \mathbf{P}_o \\ \mathbf{P}_i \end{Bmatrix}^N \quad (8)$$

where \mathbf{M} , \mathbf{C} , and \mathbf{K} are the mass, damping and stiffness matrices, respectively. The vectors $\ddot{\mathbf{u}}_o^N, \dot{\mathbf{u}}_o^N$ and \mathbf{u}_o^N contain the nodal acceleration, velocity, and displacement, respectively. Again, using the subscript i for the interface nodes and s for the surface nodes of the boundary element domain, equation (7) can be written as:

$$\begin{bmatrix} \mathbf{U}_{ss}^1 & \mathbf{U}_{si}^1 \\ \mathbf{U}_{is}^1 & \mathbf{U}_{ii}^1 \end{bmatrix} \begin{Bmatrix} \mathbf{t}_s \\ \mathbf{t}_i \end{Bmatrix}^N = \begin{bmatrix} \mathbf{T}_{ss}^1 & \mathbf{T}_{si}^1 \\ \mathbf{T}_{is}^1 & \mathbf{T}_{ii}^1 \end{bmatrix} \begin{Bmatrix} \mathbf{u}_s \\ \mathbf{u}_i \end{Bmatrix}^N + \begin{Bmatrix} \mathbf{E}_s \\ \mathbf{E}_i \end{Bmatrix}^N \quad (9)$$

Employing the traction free conditions on the surface, and solving for the interface node variables, the following expressions can be derived:

$$[\mathbf{K}_b] = [\mathbf{U}_b]^{-1} [\mathbf{T}_b], \quad [\mathbf{U}_b] = [\mathbf{U}_{ii}^1] - [\mathbf{T}_{is}^1] [\mathbf{T}_{ss}^1]^{-1} [\mathbf{U}_{si}^1], \quad [\mathbf{T}_b] = [\mathbf{T}_{ii}^1] - [\mathbf{T}_{is}^1] [\mathbf{T}_{ss}^1]^{-1} [\mathbf{T}_{si}^1] \quad (10)$$

$$\{\mathbf{E}_{bu}\}^N = [\mathbf{U}_b]^{-1} \{\mathbf{E}_b\}^N, \quad \{\mathbf{E}_b\}^N = [\mathbf{T}_{is}^1] [\mathbf{T}_{ss}^1]^{-1} \{\mathbf{E}_s\}^N - \{\mathbf{E}_i\}^N \quad (11)$$

$$\{\mathbf{t}_i\}^N = [\mathbf{K}_b] \{\mathbf{u}_i\}^N - \{\mathbf{E}_{bu}\}^N \quad (12)$$

In order to impose the compatibility and equilibrium conditions along the interface, equation (12) is to be expressed in a force-displacement relation. Therefore, the principle of virtual work is used to obtain the nodal forces from the distributed traction over each boundary element. Through these procedure, a global transformation matrix \mathbf{A} for the whole system can be assembled. The nodal forces are obtained as:

$$\{\mathbf{P}_{bb}\}^N = [\mathbf{A}] \{\mathbf{t}_i\}^N = [\mathbf{K}_{bb}] \{\mathbf{u}_i\}^N - \{\mathbf{F}_b\}^N \quad (13)$$

$$[\mathbf{K}_{bb}] = [\mathbf{A}] [\mathbf{K}_b], \quad \{\mathbf{F}_b\}^N = [\mathbf{A}] \{\mathbf{E}_{bu}\}^N \quad (14)$$

Applying the principle of weighted residuals along the interface, the coupled equation of motion is obtained as:

$$\begin{bmatrix} \mathbf{M}_{oo} & \mathbf{M}_{oi} \\ \mathbf{M}_{io} & \mathbf{M}_{ii} \end{bmatrix} \begin{Bmatrix} \ddot{\mathbf{u}}_o \\ \ddot{\mathbf{u}}_i \end{Bmatrix}^N + \begin{bmatrix} \mathbf{C}_{oo} & \mathbf{C}_{oi} \\ \mathbf{C}_{io} & \mathbf{C}_{ii} \end{bmatrix} \begin{Bmatrix} \dot{\mathbf{u}}_o \\ \dot{\mathbf{u}}_i \end{Bmatrix}^N + \begin{bmatrix} \mathbf{K}_{oo} & \mathbf{K}_{oi} \\ \mathbf{K}_{io} & \mathbf{K}_{ii} + \mathbf{K}_{bb} \end{bmatrix} \begin{Bmatrix} \mathbf{u}_o \\ \mathbf{u}_i \end{Bmatrix}^N = \begin{Bmatrix} \mathbf{P}_o \\ \mathbf{P}_i + \mathbf{F}_b \end{Bmatrix}^N \quad (15)$$

NUMERICAL EXAMPLES AND DISCUSSIONS

Validation

The three-dimensional response of an elastic half-space to a Heaviside type vertical point load is obtained. The half-space has a shear modulus $G = 99.46$ MPa and a mass density $\rho = 2$ t/m³. Figure 1(a) depicts the results and figure 1(b) displays results from literature [Neidhart, 1994, Pekeris, 1955]. Pekeris' analytical results exist only for the case of Poisson's ratio $\nu = 0.25$. Different mesh sizes are used to investigate its influence, where in figure 1(b) A represents the smallest mesh size and D the largest one. The overall behavior of the presented results is in a very good agreement with the literature solutions as shown in figure 1(b). The numerical solutions can only approximate the abrupt change of the singularity occurring at the arrival of Rayleigh waves. After the Rayleigh waves have passed, the numerical and the analytical solutions converge to the corresponding static solution.

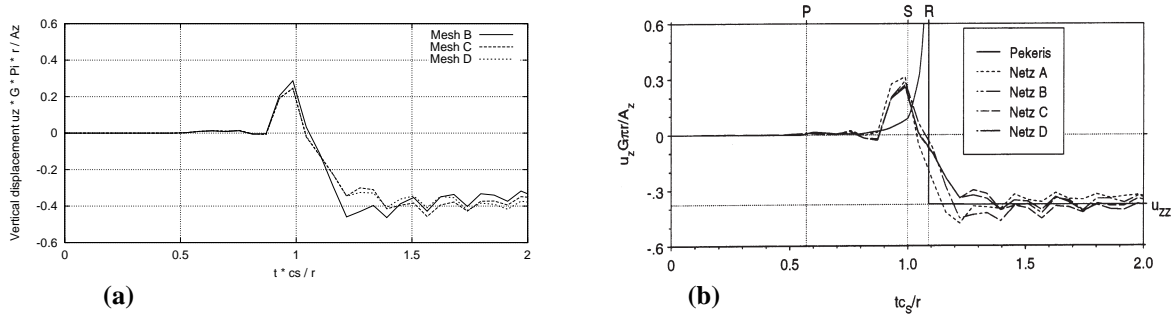


Figure 1 (a) and (b): Validation of 3-D solution. (a) present method and (b) results of Neidhart

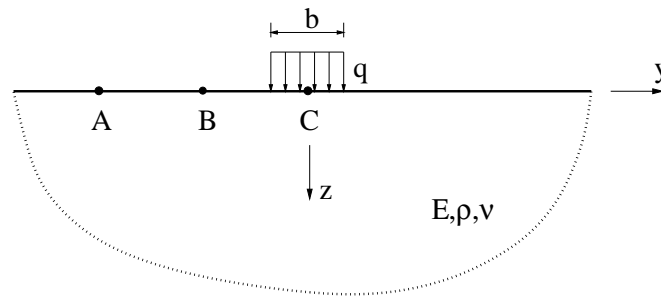


Figure 2 : Half-space under strip load

Moreover, the two methods are applied to obtain the response of an elastic half-space under a discontinues boundary stress distribution as shown in figure 2. This test example was used for comparison by many authors using different methods [Antes, 1985, Cruse and Rizzo, 1968, Mansur and Brebbia, 1982]. A vertical impulse $q = 68.95$ MPa is applied on a strip of width $b=152.4$ m. The half-space has a Young's modulus $E = 17240$ MPa, mass density $\rho = 3.15$ t/m³ and a Poisson's ratio $\nu = 0.25$. The vertical response is calculated at center of the load (point C), at distances of 152.4m and 304.8 m, point B and point A, respectively. The results of the presented methods are given in figure 3(a), while literature results are displayed in figure 3(b) [Abouseeda and Dakoulas, 1998]. Figure 3 demonstrates the good agreement of the presented results with literature solutions at all points.

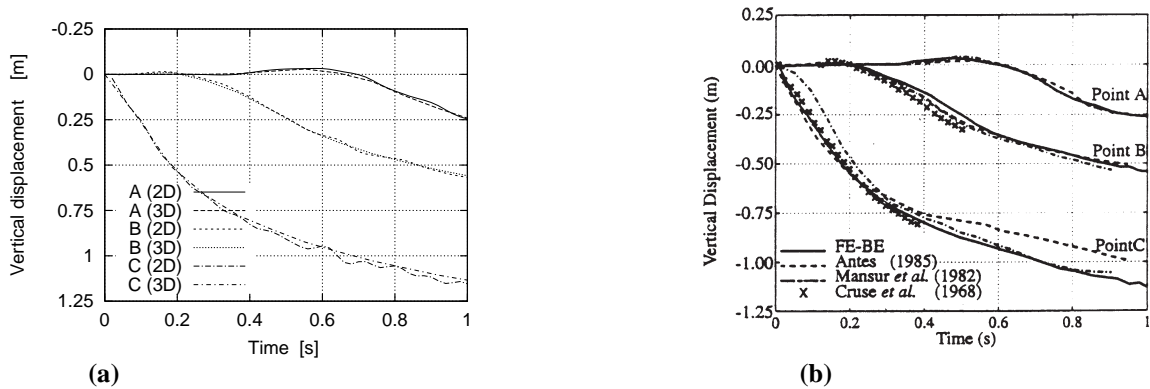


Figure 3 (a) and (b): Validation of both approaches. (a) present methods and (b) other results

Two- and Three-dimensional Responses of Half-space

According to the plane strain assumption, a two-dimensional solution assumes that the model has infinite length in the third direction. In order to find out the validity and the limitation of two-dimensional solutions, we analyze a half-space under an impulsive line load by both presented approaches. In the two-dimensional model, the y - z plane is considered and a certain part of the surface with width B is discretized. A concentrated load is applied in the middle of it. On the three dimensional model, the same width B is discretized in the y - z plane and different values of the length L in the third direction x are assumed. The half-space has a shear modulus $G = 125 \text{ MPa}$, a mass density $\rho = 2 \text{ t/m}^3$ and a Poisson's ratio $\nu = 0.25$. The case of vertical applied load is analyzed and the responses at different distances from the load along the width B are obtained. The responses at a distance of 3 m are shown in figure 4. The solid lines display the two-dimensional results, the dashed and the dotted lines give the three dimensional ones while the comparison is made in terms of the L/B ratios. It can be clearly concluded that as the ratio L/B increases, the results of both methods become close. A very good agreement is obtained for $L/B = 2.7$ for the vertical response and a good approximation is achieved for $L/B = 1.4$. For the horizontal response the best agreement is obtained for $L/B = 5.4$ or larger. The same behavior is found at other distances which are not shown here due to limited space. For applied horizontal load, the response at a distance of 3 m is shown in figure 5. In this case the agreement between the two presented methods is obtained for higher L/B -ratio, especially for the vertical responses. This may be caused by the wave scattering due to the truncated surface edges. As we have a very good agreement between the responses in the direction of the applied load some deviation in the other direction results can be accepted. Depending on these results, we can state that the problem at hand can be treated as two-dimensional if the length to width ratio L/B is not less than 3. For ratios less than 1.5, the problem has to be treated as three-dimensional.

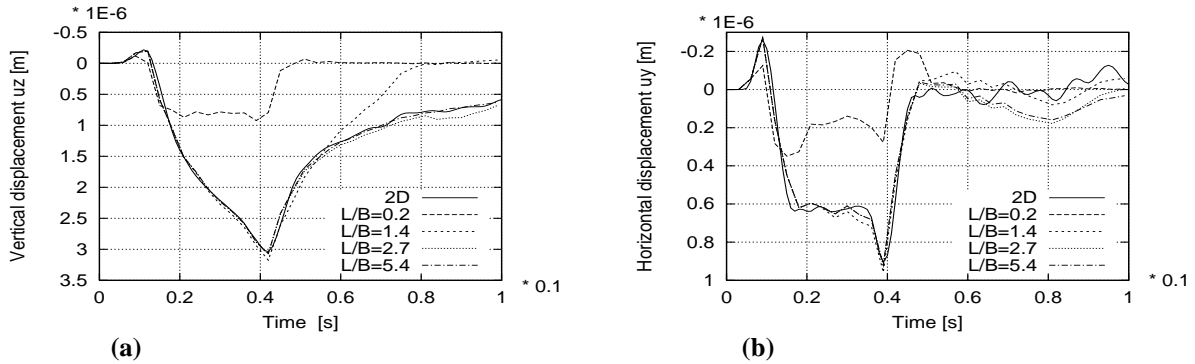


Figure 4 (a) and (b): 2-D and 3-D responses at a distance of 3m due to a vertical impulse.

(a) Vertical (b) Horizontal

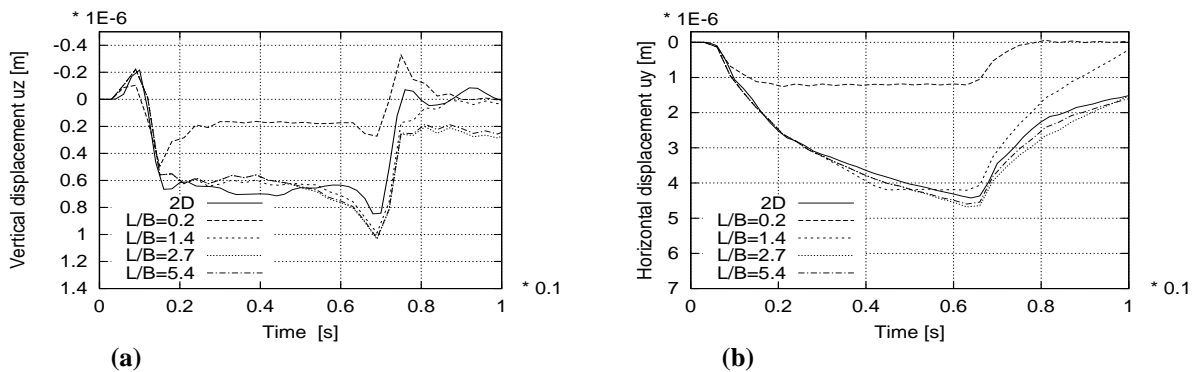


Figure 5 (a) and (b): 2-D and 3-D responses at a distance of 3 m due to a horizontal impulse.

(a) Vertical (b) Horizontal

3.3 Transient Response of a Train-Track Embankment on a Half-space

The responses of half-space to stationary train track loading is investigated. Figure 6 shows the configuration and the dimensions of the considered train track embankment model. The 0.8 m thick embankment layer is assumed to be resting on a uniform half-space. The train track load is represented by two concentrated impulsive line loads with unit amplitude (1 kN/m) and lasts for 0.02 seconds. The mass density $\rho = 2 \text{ t/m}^3$ and the Poisson's ratio $\nu = 0.33$ are assumed to be identical for the embankment and the half-space in all cases. Different values for the shear wave velocity v_s are assumed for five cases as given in table 1. To grasp the wave propagation characteristics in the embankment layer and through the half-space, the responses at four different locations, A, B, C, and D (figure 6) are obtained.

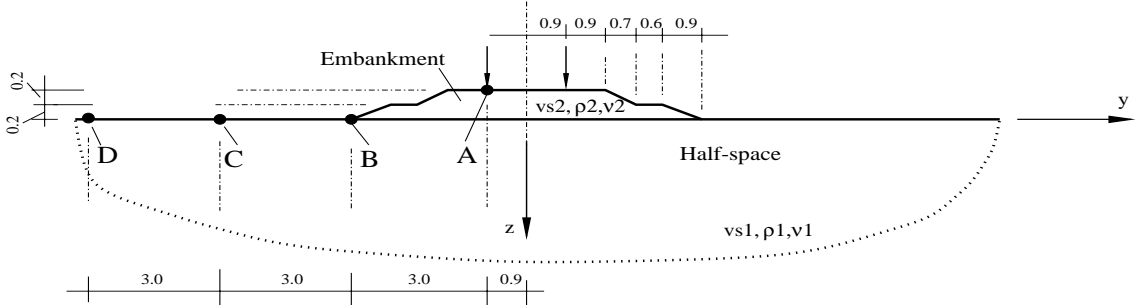


Figure 6: Train track embankment on half-space model

Case 1 which will be used as a reference case hereafter, is analyzed by both methods. The responses at a distance of 1.5 m from the track center are shown in figure 7. Although the embankment has an irregular surface and relatively low L/B ratios were used, the good agreement between both results can be clearly concluded and confirms our previous finding. The time histories of vertical responses at the selected four locations from the two-dimensional analysis are shown in figure 8, for Case 1 and Case 2. The time delay and the maximum amplitude decrease with increasing distance can be clearly depicted for both cases. The slight effect of the wave scattering at the embankment edges for Case 1 is observed, while in Case 2 a larger effect can be concluded due to the wave scattering by the subsurface between the embankment and the half-space. As the half-space has more rigidity in Case 2, the maximum responses at all locations are reduced to about 50% to 60% of the responses in Case 1. The time histories of vertical and horizontal responses at locations A and C for all cases are shown in figures 9 and 10, respectively. It is clear that Case 4 which represents a very weak embankment layer on more rigid half space gives the highest response on the embankment and the lowest response along the half-space surface (figure 11). Moreover, the embankment layer continues to vibrate after the load ended with its fundamental frequency similar to a case of single layer on a base rock (figure 9). Although the half-space surface has the lowest response, the vibration continues after the end of the load due to the wave radiation from the vibrating embankment layer (figure 10). On contrast, when the half-space is less rigid than the embankment (Case 3), higher responses result at the embankment, with high amplification, especially in horizontal direction. The maximum response time is delayed because of the low wave speed in the half-space (figures 10 & 11). In Case 5, where a relatively rigid embankment is used, reduced responses result at the embankment with slight reduction in the response along the surface at other locations. Therefore, it can be stated that a more rigid half-space results in smaller responses under the condition that the stiffness ratio between the half-space and the embankment layer is not so large in such a way that the embankment behaves as a fixed base layer. It can also be concluded that Case 2 presents the best solution for the model under consideration. But it should be mentioned that a more detailed parameter study is required in practice for design of train track embankment, according to the available site conditions.

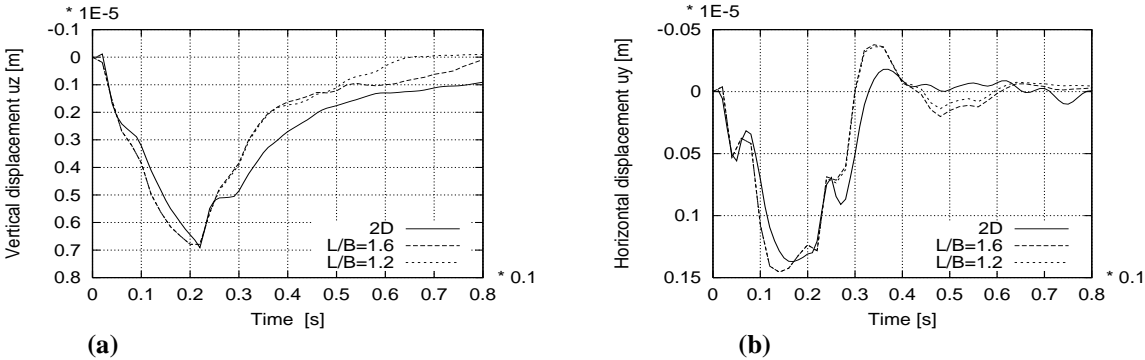


Figure 7 (a) and (b): 2-D and 3-D responses at a distance of 1.5 m. (a) Vertical and (b) Horizontal

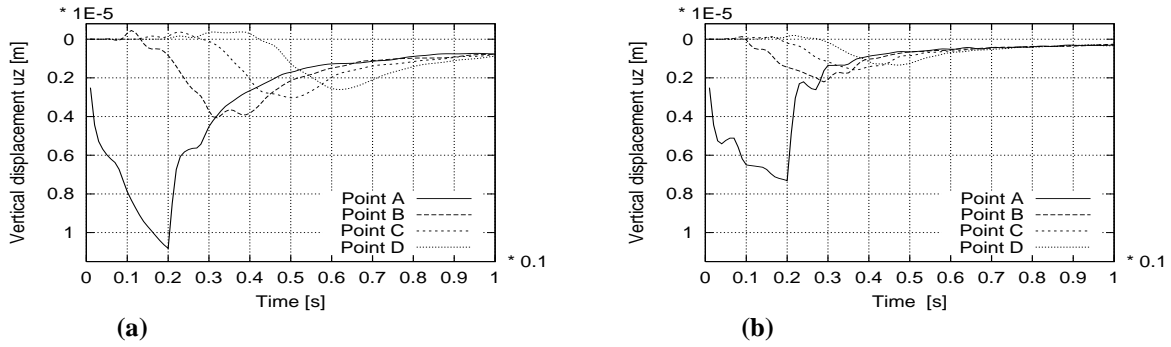


Figure 8 (a) and (b): Vertical responses at different locations. (a) Case 1 and (b) Case 2

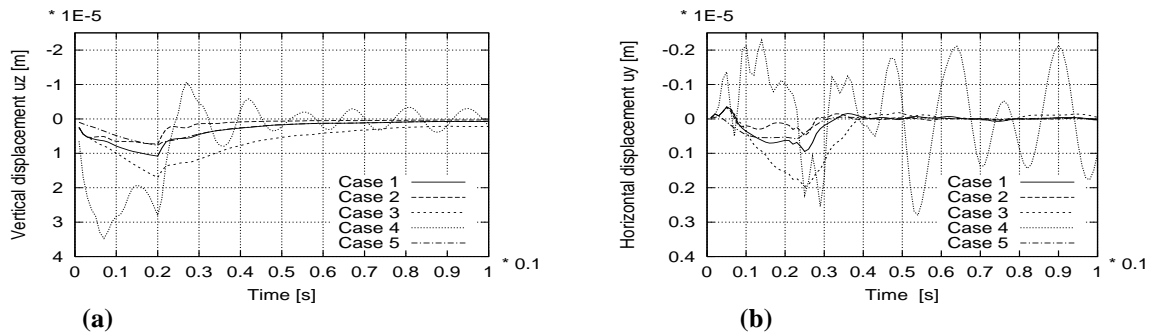


Figure 9 (a) and (b): Responses at location A. (a) Vertical and (b) Horizontal

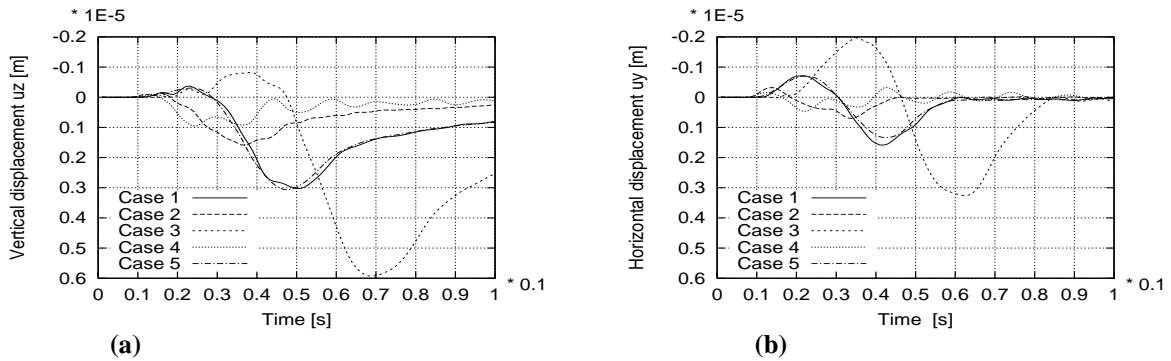


Figure 10 (a) and (b): Responses at location C. (a) Vertical and (b) Horizontal

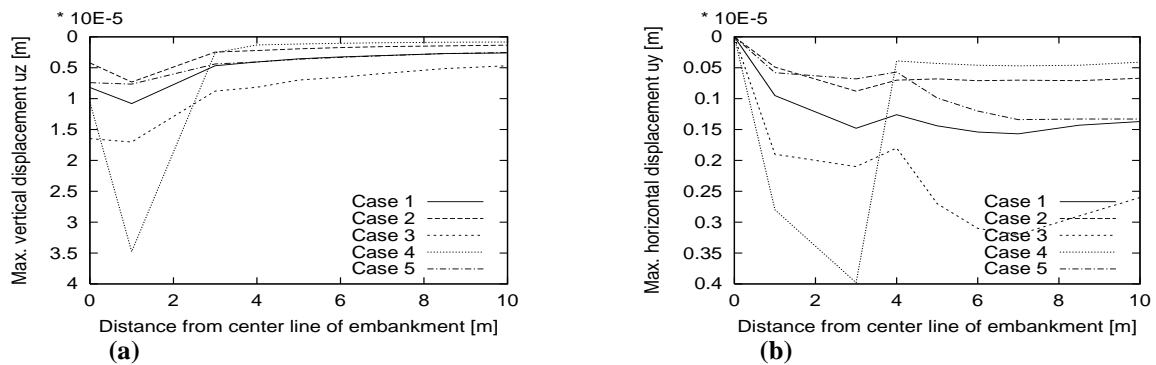


Figure 11 (a) and (b): Maximum responses along the surface. (a) Vertical and (b) Horizontal

Table 1: Shear wave velocity v_s (m/s) of embankment and half-space at different cases

	Case 1	Case 2	Case 3	Case 4	Case 5
Embankment	250	250	250	100	500
Half-space	250	400	150	600	250

CONCLUSIONS

Two modelling approaches for the analyses of half-space subjected to dynamic loads and train track loads are presented in time domain. The validity of each approach is demonstrated using results from literature. The comparison between results of the two methods point out that a problem can be assumed as two-dimensional if the length to width ratio L/B is not less than 3. If the ratio is less than 1.5 the three-dimensional solution is essential. For the problem of wave propagation in the train track embankment and the underlying half-space, a detailed parameter study has to be performed.

ACKNOWLEDGEMENT

Thanks are given to the Graduiertenkolleg “*Computational Structural Dynamics*” funded by the German Research Foundation (DFG) for the support of the first author’s research stay at the Ruhr University Bochum, and the second author’s scholarship. Furthermore, the first and the second authors would like to express their gratitude to the third author for his continuous support and kind cooperation.

REFERENCES

- Abouseeda, H., and Dakoulas, P., (1998), “Non-linear dynamic earth dam-foundation interaction using BE-FE method”, *Earthquake Engng. Struct. Dyn.*, 27, pp917-936.
- Antes, H., (1985), “A boundary element procedure for transient wave propagation in two-dimensional isotropic elastic media”, *Finite Element Anal. Des.*, 1, pp313-323.
- Chua, K.H., Balendra, T. and Lo, K.W., (1992), “Ground borne vibrations due to trains in tunnels”, *Earthquake Engng. Struct. Dyn.*, 21, pp445-460.
- Cruse, T.A., and Rizzo, F.J., (1968), “A direct formulation and numerical solution of the general transient elastodynamic problem 1”, *Int. J. Math. Anal. Appl.*, 22, pp244-259.
- Gaul, L., Schweizer, B., (1998), Analytische Berechnung der integralfreien Terme aus den Somigliana Identitäten. University of Stuttgart, Germany, Sonderforschungsbereich 404, Mehrfeldprobleme der Kontinuumsmechanik, Report 98/01.
- Guiggiani, M., (1992), “Computing principal value integrals in 3-D BEM for time-harmonic elastodynamics - a direct approach”, *Communications in Applied Numerical Methods*, Vol. 8, pp141-149.
- Jones, C.J.C., (1994), “Use of numerical models to determine the effectiveness of anti-vibration systems for railways”, *Proceedings of the Institution of Civil Engineers, Transportation*, 105, pp43-51.
- Jones, C.J.C., and Block, J.R., (1996), “Prediction of ground vibration from freight trains”, *Journal of Sound and Vibration*, 193, 1, pp205-213.
- Krylov, V.V., (1995), “Generation of vibration by superfast trains” *Applied Acoustic*, 44, pp149-164.
- Li, H.B., Guo-Ming, H., (1985), “A new method for evaluating singular integrals in stress analysis of solids by the direct boundary element method”, *Int. J. Num. Meth. in Eng.*, 21, pp2071-2098.
- Mansur, W.J. and Brebbia, C.A., (1982), “Formulation of the boundary element method for transient problems governed by the scalar wave equation”, *Appl. Math. Modelling*, 6, pp307-311.
- Neidhart, T., (1994), *Lösung dreidimensionaler linearer Probleme der Bodendynamik mit der Randelementmethode*, Veröffentlichungen des Institutes für Bodenmechanik und Felsmechanik, University of Karlsruhe, Germany.
- Pekeris, C.L., (1955), “The seismic surface pulse”, *Proceedings of the National Academy of Sciences*, 41, 469.
- Pflanz, G., (1999), “Wellenausbreitung in elastischen Kontinua infolge sich bewegender Lasten”, *Graduiertenkolleg “Computational Structural Dynamics” an der Ruhr-Universität Bochum. Tagungsband zum Abschlußkolloquium. Fortschrittsberichte VDI, Reihe 18*, Düsseldorf, Germany, (to appear)
- Stokes, G.G., (1849), “On the dynamical theory of diffraction”, *Trans. Cambridge Philos. Soc.*, 9, pp793-797.
- Yoshioka, O. and Ashiya, K., (1990), “Effect of masses and axle arrangements of rolling stock on train induced ground vibrations”, *Quarterly review of RTRI.*, 31, 3, pp145-152.